

Cooling limits on galaxy formation

Gas dynamical simulations incorporating a background UV field and metal enrichment

Daniel Källander and John Hultman

Uppsala Astronomical Observatory, Box 515, S-751 20 Uppsala, Sweden (e-mail: pohlman@astro.uu.se)

Received 26 February 1997 / Accepted 25 November 1997

Abstract. We present hydrodynamical simulations of the formation of galaxies in the mass range $10^9 - 10^{13} M_{\odot}$, with the focus on the efficiency of gas cooling.

The effect of a background UV radiation field, and the effect of metal enrichment of halo gas due to star formation and stellar evolution, are investigated. A background radiation field is found to strongly suppress the formation of galaxies with circular velocities less than ≈ 50 km/s. The effect is, however, not large enough to reconcile hierarchical clustering models with observations.

Metal enrichment of the halo gas increases the cooling rate at low redshifts. We find that the mass fraction of gas at virial temperatures may be reduced by a factor of two, in simulations with a UV background field added. The decrease in overall efficiency of gas cooling due to the inclusion of a UV background field can be more than compensated for by the increased cooling that follows metal enrichment of halo gas, but the effect may depend strongly on the assumed model of metal enrichment.

Key words: galaxies: formation – cooling flows – hydrodynamics – methods: numerical

1. Introduction

It is generally believed that galaxies formed by gravitational collapse. Small fluctuations in the primeval density field grew through gravitational instabilities. When the mean density in a proto-galaxy reaches approximately twice the mean density of the Universe, the proto-galaxy breaks away from the general expansion of the Universe and collapses, and forms a gravitationally bound galactic halo. If the gas in a galactic halo is able to cool efficiently, it can dissipate kinetic energy and condense into a galactic object at the center of the halo.

The purpose of this paper is to study under what circumstances the gas in proto-galaxies is able to cool efficiently, and condense into objects with galactic densities. Particularly, we take a close look at the possible effects of a strong background

UV radiation field and the dynamical effects of metal enrichment of halo gas. The results are based on three-dimensional hydrodynamical computer simulations, and a standard CDM cosmology is assumed throughout. The results should have some relevance for all hierarchical scenarios of galaxy formation.

In hierarchical models of galaxy formation, the statistical cosmological time of collapse for a proto-galaxy is an increasing function of mass. More massive galactic halos thus form later. This general picture is consistent with observations indicating that clusters are younger than the contained galaxies, and that the Universe is homogeneous on very large scales.

Any theory of galaxy formation must address fundamental properties of the observed galaxy population like characteristic masses and sizes. Rees & Ostriker (1977), and Silk (1977), showed that the characteristic masses and sizes of galaxies are just those to be expected of gas clouds that can cool in a Hubble time. This provides a natural explanation for the sharp upper cut-off in the galaxy luminosity function; more massive proto-galaxies can not cool in a Hubble-time. These calculations were based on simple models of homogeneous gas clouds, very unlike the highly inhomogeneous collapse of a proto-galaxy in a hierarchical model, where objects are formed by merging of smaller ones, where the gas have already had time to cool. If a substantial fraction of the gas is still heated to virial temperatures, these models still shows that limits due to gas cooling are likely to play an important role in the formation of galaxies.

Observations suggest that only a small fraction, around 1 – 2 %, of the closure density of the Universe is in the form of stars. It therefore seems likely that most of the baryonic matter has avoided falling into compact objects, where efficient star formation could take place. Hierarchical models (White & Frenk 1991, Cole et al. 1994), on the other hand, tend to lock up most of the baryonic mass in the universe in small galactic objects, at early times. If the gas in these halos is able to cool and condense into dwarf galaxies, hierarchical models seem to overpredict the current mass fraction of stars in the Universe. One possible explanation is that supernova driven winds are able to suppress the formation of dwarf galaxies (Dekel & Silk 1986). Another process that may be important involves the presence

of a photo-ionizing UV background radiation field. A photo-ionizing background field would heat the gas, and, by keeping the gas at a high degree of ionization, it would suppress collisional line cooling from neutral atoms. Evidence for such a field is given by the lack of a Gunn-Peterson effect even at high redshifts $z \approx 5$ (Webb et al. 1992), indicating that the Universe was highly ionized at these redshifts.

Based on simple models of the collapse of gas clouds, Efstathiou (1992) argued that a strong background UV radiation field might indeed suppress the formation of dwarf galaxies. The gas is heated by photo-ionization, and the gas is also kept at a high degree of ionization that suppresses collisional line cooling. Efstathiou found that this might prevent the gas in galactic halos with circular velocities less than 50 km/s from cooling.

The UV background photo-ionization heating is able to raise the equilibrium gas temperature to only about $10^4 - 10^5 \text{ K}$, for the typical range of densities in question, ($n_H = 10^{-6} - 10^{-2} \text{ cm}^{-3}$). Further, the photo-ionization process is proportional to the density, through relative abundances, but the excitation and collisional cooling processes are proportional to the density squared. Therefore, the effect of photo-ionization is larger for low densities, and becomes less significant for higher densities. Above $10^5 - 10^6 \text{ K}$ photo-ionization effects also diminishes, due to first hydrogen, later helium, becoming completely ionized. It is therefore only likely to be important for the dynamics of small galaxies. But, large galaxies could also have been affected, since their lower mass progenitors may have been unable to cool.

Typical virial temperatures of galactic halos are $10^4 - 10^6 \text{ K}$. In this temperature range the cooling rate of interstellar gas is highly dependent on the metallicity. The cooling rate of a gas with solar metallicity can be more than one order of magnitude larger than for a gas of primordial composition (Sutherland & Dopita 1993). Observations of intra-cluster gas typically indicates metallicities of $[\text{Fe}/\text{H}] = -0.4$. This metal enrichment can have a strong effect on the amount of gas that is able to cool at low redshifts.

Källander (Källander (1996)) has performed simulations similar to the ones presented here, using a similar model for the metal enrichment of halo gas, (described in the next section), but twice as high metallicity yield. The numerical resolution was similar, but no UV field was included, and only galaxies with a total mass of $10^{12} M_\odot$ were studied. The increase in cooling rate, due to line cooling in metals, was in that case found to be enough to cause the hot halo gas to collapse in a cooling flow, in roughly one Hubble time. Without the increased cooling rate, significantly less cooling flow was present, and essentially no disk formed. Some experimentation seems to indicate that the magnitude of the gas dynamical effects of metal enrichment, are sensitive to the details of how the metal enrichment is modelled.

White and Frenk (1991) used an intricate semi-analytic framework to compare different models of hierarchical galaxy formation to observations, and found that the results were sensitive to the assumptions made for the metal enrichment of the gas.

Other simulations including the effects of photo-ionization have been presented by Vedel, Hellsten, & Sommer-Larsen (1994), Thoul & Weinberg (1996), Quinn, Katz, & Efstathiou (1996), Weinberg, Hernquist, & Katz (1997), Navarro & Steinmetz (1997). These authors uses different implementations, initial conditions and strengths of the photo-ionizing field. Vedel et al. uses three dimensional SPH simulations of a Milky Way sized object, but cannot draw conclusions on objects of other masses. Thoul & Weinberg uses one dimensional models, and have much higher resolution. The remaining uses 3D SPH simulations and emphasise on resolution effects, which are shown to be of critical importance to the results in these simulation. In spite of that these authors uses different implementations, the main conclusions are very similar. A background photo-ionizing field does have some effects on lower mass objects, but cannot alone be responsible for suppressing the formation of dwarf galaxies, and make the hierarchical CDM models consistent with observations. These authors does not include the effects of metal enrichment, but this does not alter the general result, however.

Hierarchical clustering is a highly inhomogeneous process. Direct three-dimensional simulations are therefore a vital complement to lower dimensional analytical models. Gas dynamics must be included because dissipation is a fundamental part of galaxy formation. In this article we present computer simulations of galaxy formation that provide further insight on hierarchical clustering models, with an emphasis on cooling arguments. Even though a CDM cosmological model is assumed throughout, the results should have some relevance for all hierarchical scenarios. The effects of a UV background is investigated by running otherwise identical simulations, with and without the effects of an ionizing field incorporated. To be able to address questions about the mass dependence of physical processes, simulations covering a wide range of galactic masses are presented.

2. Simulations

The simulations presented here follow the evolution of two fluids: a collision-less component that comprises 95% of the mass and represents the dark matter, and a second hydrodynamical gas component. Gravitational forces are calculated using a tree code and the hydrodynamical equations are solved for the gas by use of the smooth particle hydrodynamics (SPH) method. Details of the implementation can be found in Hultman & Källander (1997).

The gas consists of hydrogen and a 24% mass fraction of helium, typical of estimated primordial values. Furthermore, we assume that the gas is optically thin and in ionization equilibrium at all times. The most important cooling processes are radiative cooling by bound-bound and bound-free transitions. Compton cooling by electron scattering against the Cosmic Microwave Background (CMB) can also have a significant effect at high redshifts, but at low redshifts, $z < 4$, the photon density of the CMB is too low to lead to any significant Compton cooling.

In some of the simulations an external strong UV radiation background field is present. The time evolution of this field is fixed already at the start of the simulations, and does not depend on the state of the gas in the simulated region. This field changes the gas cooling rate, and adds a redshift dependence to the cooling function. The gas is also heated by this field.

Radiative molecular cooling is not included, and this limits us when choosing objects to study. Below $\approx 5 \times 10^3$ K, atomic radiative cooling is inefficient and molecular radiative cooling may be important. By neglecting molecular cooling we cannot with any certainty simulate systems where the gas pressure at temperatures below 10^4 K can be dynamically important. This implies a lower mass limit on the applicability of these simulations.

Neutral gas of primordial abundance is stable against collapse in a dark matter halo if the halo mass, M_{halo} , is (Rees 1986, Quinn et al. 1996)

$$M_{halo} < 1.09 \times 10^9 \left(\frac{T}{10^4 \text{K}} \right)^{3/2} \times h_{50}^{-1} (1+z)^{-3/2} \left(\frac{\mu}{m_p} \right) M_{\odot}. \quad (1)$$

T , m_p , μ , z , h_{50} are respectively the gas temperature, the proton mass, the gas mean molecular weight, the formation redshift and the Hubble constant in units of $\text{km s}^{-1} \text{Mpc}^{-1}$. For a neutral gas, $T \sim 10^4$ K, and a formation redshift of $z = 3$ this corresponds to a mass of $1.25 \times 10^8 M_{\odot}$. A further complication at these mass scales is that galactic halos with as low masses as $10^8 M_{\odot}$ are very susceptible to disruption by supernovae (Dekel & Silk 1986). The least total mass in the sequence of simulations, was for these reasons chosen to have a total mass of $10^9 M_{\odot}$.

Each object was simulated both with and without a photo-ionizing background, using the same initial density field. In this way it is possible to investigate the effects of the photo-ionizing background, without making a statistical study that would require a large number of simulations. The assumed background radiation field is of the form

$$J(\nu) = J_{-21}(z) \times 10^{-21} (\nu_L/\nu) \text{ erg cm}^{-2} \text{sr}^{-1} \text{Hz}^{-1} \text{s}^{-1}, \quad (2)$$

where ν_L is the Lyman limit frequency, and the time dependence of the field is contained in the function $J_{-21}(z)$.

Observational determinations of $J_{-21}(z)$ in recent years include the following (Haardt and Madau 1996): $\log J_{-21} \approx 0.5$ at $1.6 < z < 4.1$ (Bechtold 1994), $-1.0 < \log J_{-21} < -0.5$ at $z \approx 4.2$ (Williger et al. 1994), $\log J_{-21} = 0.0 \pm 0.5$ at $1.7 < z < 3.8$ (Bajtlik et al. 1988, Lu et al. 1991), and $\log J_{-21} = -0.3 \pm 0.2$ at $1.7 < z < 3.8$ (Espey 1993). A decline in the intensity is expected at high redshifts due to a decline in the number density of quasars and increased absorption by Lyman-alpha clouds. Here $J_{-21}(z)$ is taken to have the form

$$J_{-21}(z) = \begin{cases} 4/(1+z) & 3 < z < 6 \\ 1 & 2 < z < 3 \\ z-1 & 1 < z < 2. \end{cases} \quad (3)$$

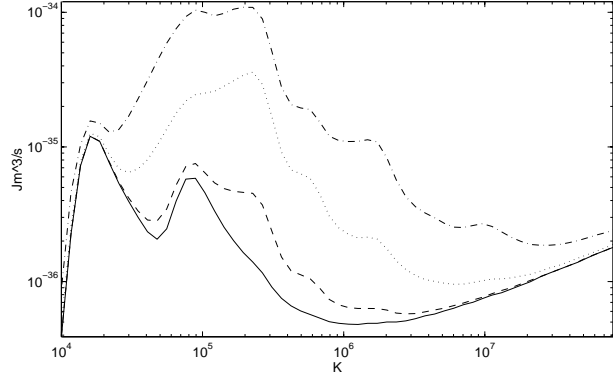


Fig. 1. The normalized cooling function as given by Sutherland & Dopita. Different curves correspond to different gas metallicity, zero metallicity ($[\text{Fe}/\text{H}] = -3$, solid curve), $[\text{Fe}/\text{H}] = -2$ (dashed curve), $[\text{Fe}/\text{H}] = -1$ (dotted curve) and $[\text{Fe}/\text{H}] = 0$ (dot-dashed curve). ($[\text{Fe}/\text{H}]$ being the value of the logarithm of the metal content normalized to the solar value.)

Proto-galactic gas is enriched with metals ejected from heavy stars, through stellar winds and supernovae. This leads to an significant increase in the gas cooling rate at the temperatures that are relevant for galaxy formation, as can be seen from cooling curve by Sutherland & Dopita (1993), in Fig. 1. To take cooling effects of metals into account, a description of the star formation rate is necessary. Star formation is, however, not well understood. Since the only purpose here is to roughly estimate the amount of heavy metals ejected, a simple description is adequate.

All gas with a density contrast above 200 is taken to be inside “collapsed structures”, and gas inside such collapsed structures is assumed to be transformed completely into stars. This is only made for the purpose of estimating the average gas metallicity in the proto-galaxy; dynamically, baryonic mass remains gaseous everywhere. Instantaneous recycling is also assumed (heavy stars eject their metals immediately after being formed) and complete mixing of the metals throughout the proto-galaxy (making the gas metallicity homogeneous) which simplifies the model further. The gas metallicity is then given by (Tinsley 1980)

$$Z(t) = y \ln M/(M - M_s(t)) \quad (4)$$

where Z , y , M , M_s and t are, respectively, gas metallicity, yield, total baryonic mass, total mass in stars and time. That is, the average gas metallicity in the proto-galaxy, is only dependent of the average gas fraction in the proto-galaxy, (the proto-galaxy being the entire simulation volume in this context). Here a yield $y = 0.5 Z_{\odot}$ is adopted, which was found to give a gas metallicity in accordance with observed values.

Assuming a time evolution and spectral shape for the background field, a four dimensional table in redshift, metallicity, density and temperature was calculated for both the cooling and heating. We used the publicly available program CLOUDY (Ferland 1993) to calculate cooling and heating tables. The tables were stored in a file and subsequently read in at the begin-

ning of each simulation. Linear interpolation was then used to calculate heating and cooling rates during the simulation.

3. Initial conditions

In setting up initial conditions for a simulation it is necessary to specify the cosmological model. Here a CDM model, with a baryon fraction of 5%, a bias parameter of $b = 1.5$, $\Omega = 1$, $\Lambda = 0$, and a Hubble constant $h = 0.5$ in units of 100 km/s/Mpc, is employed. The main significance of the cosmological model is in this case to provide a normalization, and shape, of the power spectrum of density fluctuations. The amplitude of the power spectrum on galactic scales is constrained by observations, choosing $\sigma_8 = 1/b$, (the rms field value, smoothed with a top hat filter on a scale of $8/h$ Mpc). Choosing another hierarchical cosmological model is therefore likely to have only moderate effects on the results of these simulations.

The simulations presented here cover a mass range of objects, $10^9 - 10^{13}M_\odot$, in order to address questions about the mass dependence of different physical mechanisms. The gas is initially represented by 8000 particles and the dark matter by 4000 particles. Gas particles are under certain conditions allowed to merge with other nearby gas particles, and the number of gas particles is therefore a decreasing function of time, (see Hultman & Källander 1997 for details). The simulations start with a spherical region of the Universe at a redshift of $z = 30$.

We choose the simulation volumes as spheres, containing precisely the mass of the object in question. This minimizes the volume needed to be simulated, reducing costs in computational time, allowing for highest possible resolution, which is of critical importance in these type of simulations. The initial conditions used here are similar to the ones used by Katz & Gunn (1991), but there are some important differences, and improvements as will be explained below.

Selecting a limited spherical region to study the formation of a galaxy leads to two major complications, the neglect of the surroundings and the selection of a proper site.

Galaxies do not form at random locations. Finding good candidates for galactic seeds at high redshifts, using only the density distribution as a guide, is a difficult task. One possible procedure is to make a low resolution simulation of a large region, and thereby identify the sites where galactic halos of the desired type form. After that, such a region can be re-simulated with higher resolution. Although cumbersome, this is feasible and has been done (Navarro & White 1994).

We chose instead to rely on the “peaks formalism” (Bardeen et al. 1986) to identify likely sites of the formation of galactic halos. This enables us to use an explicit scheme where key properties of the proto-galaxy can be specified, “seeding” the formation of the galactic object to form at the desired location. The details of this are described in Appendix A.1.

By ignoring the surrounding regions outside the proto-galaxy, no account is taken of tidal interactions. Tidal interactions with the surrounding matter is believed to be what gives galaxies their spin. In its early pre-collapse phase, the proto-galaxy acquires angular momentum through gravitational inter-

Table 1. Simulation parameters.

Total mass [M_\odot]	r_{init} [Mpc]	V_{circ} [km/s]	ϵ_g [kpc]	ϵ_{DM} [kpc]	T_{vir} [K]
10^9	0.15	28	0.37	1.0	$2.85 \cdot 10^4$
10^{10}	0.33	55	0.74	2.0	$1.10 \cdot 10^5$
10^{11}	0.71	100	1.1	3.0	$3.63 \cdot 10^5$
10^{12}	1.52	170	1.5	4.0	$1.05 \cdot 10^6$
10^{13}	3.27	330	2.2	6.0	$3.95 \cdot 10^6$

actions with surrounding matter. Density fluctuations grow by gravitational instabilities and at some time the proto-galaxy collapses. When it collapses, the quadrupole, and higher, moments of its mass distribution diminish as it shrinks in size. This drastically reduces any tidal interactions, and the angular momentum accumulated in the pre-collapse phase is effectively frozen in at this time. It is therefore believed that a galaxy that has not been involved in any major merger events has had an almost constant angular momentum since the main collapse of the proto-galaxy.

Thus, to approximate the neglected effects of the proto-galactic surroundings, the simulated spherical region is started in solid body rotation. The amount of angular momentum added corresponds to a spin parameter of $\lambda = 0.05$ (Barnes & Efstathiou 1987).

4. Primordial gas simulations

A first series of simulations does not include a UV field, nor metal enrichment of gas. The gas has a primordial composition, with a 24% mass fraction of helium, and the rest of the mass in hydrogen.

All the simulations in this series result in the formation of a single dominant collapsed gas object at $z = 0$, which contain more than 90% of the collapsed gas mass. This object is built up through hierarchical merging of smaller objects. The mass of the most massive progenitor as a function of redshift can be seen in Fig. 2. The redshift, at which the mass of the largest progenitor has acquired half of the final mass, is an increasing function of total proto-galactic mass. For the 10^9M_\odot simulation this redshift is $z \approx 2.2$, and for the $10^{13}M_\odot$ simulation it is $z \approx 0.2$.

During the collapse of the proto-galaxy the gas acquires kinetic energy, which is then converted into thermal energy by shocks and radiated away. In the low mass galaxies the radiative gas cooling is efficient and keeps the gas cool, as can be seen in Fig. 3. The fraction of gas that can cool depends on the redshift of formation. At high redshifts the density of the Universe is higher, and the cooling therefore stronger.

The shape of the cooling curve also gives a strong implicit redshift dependence of the efficiency of gas cooling. Radiative energy losses are highest in the temperature range $10^4 - 10^5$ K. Most gas that is shock heated to temperatures above 10^5 K stays hot for more than a Hubble time, whereas gas that is heated to less than 10^5 K experiences an order of magnitude stronger cooling and cools well within a Hubble time.

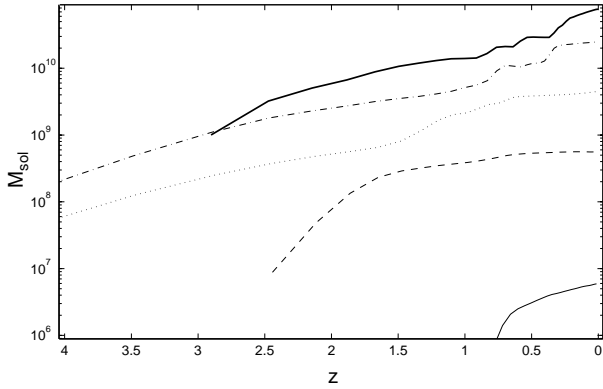


Fig. 2. The mass of the most massive progenitor, as a function of redshift, for the primordial gas simulations. The different curves represent values for simulations with different total mass: $10^9 M_\odot$ (solid), $10^{10} M_\odot$ (dashed), $10^{11} M_\odot$ (dotted), $10^{12} M_\odot$ (dot-dashed), $10^{13} M_\odot$ (fat solid).

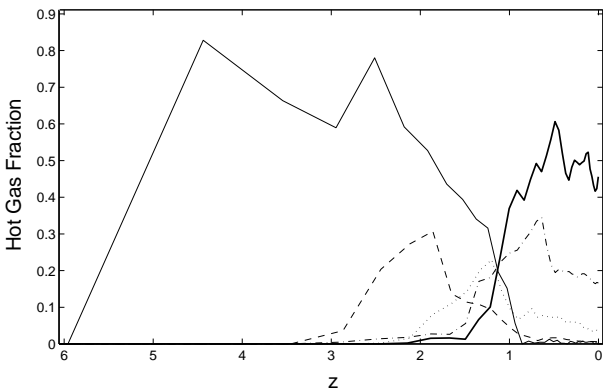


Fig. 3. The mass fraction of gas inside the virial radius that has a temperature exceeding half the virial temperature, for the primordial gas simulations. Notation as in Fig. 2.

It can be seen in Fig. 3 and Table A1 that the galactic halos that contain gas at virial temperatures at $z = 0$, are those with a virial temperature exceeding 10^5 K. These galactic halos form late, and have accumulated less than half the final mass at $z = 1$.

The gas core in the $10^{13} M_\odot$ simulation forms late, at $z \approx 0.2$, see Fig. 2, in a series of merging events. However, the hot halo remaining at $z = 0$, and containing 30% of the gas mass, forms much earlier, at $z \approx 1$. Between $z = 1$ and $z = 0.2$, several collapsed gas clumps, none of which has a mass in excess of 20% of the mass of the final gas core, share a common hot pressure supported gas halo. The gas cooling is relatively inefficient at the high temperatures of this hot halo, and there is no significant amount of cooling inflow of gas until the present epoch.

The central gas core that forms in all simulations is very compact, and is not resolved. This over-concentration of mass can be seen from the rotation curves in Fig. 4, which rise very rapidly in the innermost regions.

The galactic objects that form are very compact because the collapsed gas has lost much of the angular momentum that

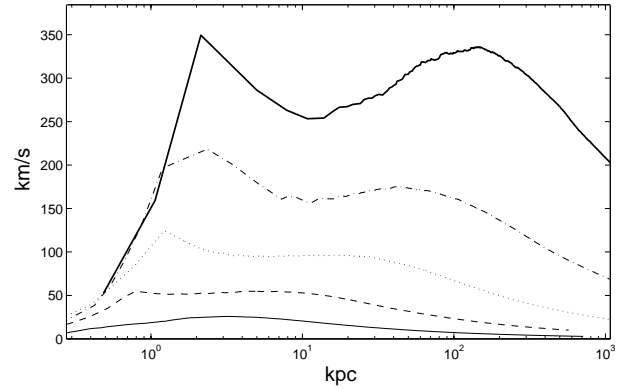


Fig. 4. Circular velocity as a function of radius, for the primordial gas simulations. Notation as in Fig. 2.

was injected at the start of the simulations. This effect is well known, and have been previously investigated by Navarro & Benz (1991), Katz & Gunn (1991), Vedel, Hellsten, & Sommer-Larsen (1994), Navarro, Frenk, & White (1995), Navarro & Steinmetz (1997), but was first found by Lake & Carlberg (1988), (using a “sticky particle” method).

The total angular momentum is in all cases conserved to well within 1%, and if the collapsed gas has lost angular momentum that angular momentum must have been transferred to the dark matter component. Fig. 5 shows the total angular momentum of the gas, normalized to the initial value. It is clear that between 10 and 90% of the gas angular momentum has been transferred to the dark matter component. In the 10^{12} and $10^{13} M_\odot$ simulations this angular momentum transfer is, however, not very pronounced. Instead, most of the gas angular momentum is contained in the hot halo of pressure supported gas that surrounds the central collapsed object. (Note that above mentioned authors considered the angular momentum of the disk, and did not include the halo.)

5. Simulations with an ionizing field

A background UV field affects the gas in two ways: (i) the gas is heated by photo-ionization; and (ii) it ionizes the gas and thereby reduces its ability to cool by collisional excitation of neutral atoms. In these simulations the background radiation field is non-zero in the range $1 < z < 6$.

The rate of photo-ionization heating by the background field is proportional to the local gas density, and the rate of cooling by collisional line radiation, the dominant cooling mechanism, is proportional to the square of the local gas density. Heating by photo-ionization is therefore most important in low density regions, where the equilibrium temperature can rise to $T \approx 3 \cdot 10^4$ K. This temperature is comparable to the virial temperature of the galactic halos that form in the $10^9 M_\odot$ and $10^{10} M_\odot$ simulations, but much less than the corresponding temperature for the largest simulations. The dynamical effects of heating should therefore be small for the largest galaxies.

Fig. 6 shows the mass fraction of gas within the virial radius that has a temperature exceeding half the virial temperature as a

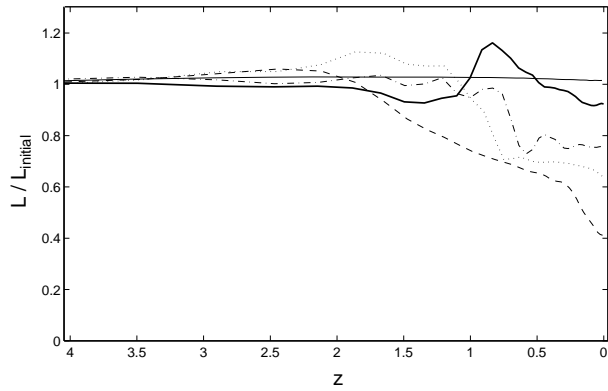


Fig. 5. Total angular momentum of the gas component, normalized to the initial value, as a function of redshift, for the primordial gas simulations. Notation as in Fig. 2.

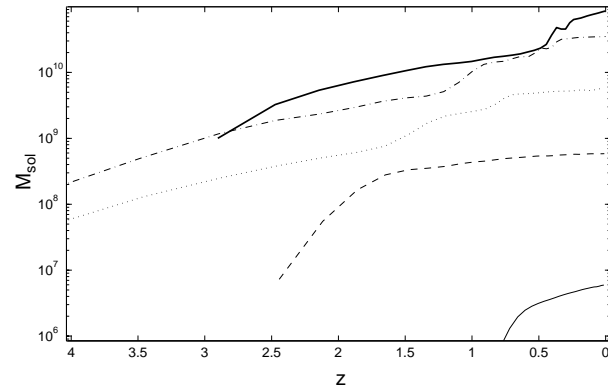


Fig. 7. The mass of the most massive progenitor, as a function of redshift, for the simulations with a background UV field. Notation as in Fig. 2.

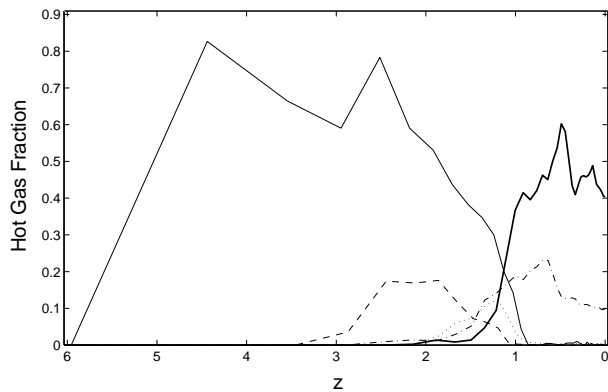


Fig. 6. The mass fraction of gas inside the virial radius that has a temperature exceeding half the virial temperature, for the simulations with a background UV field. The curves represent simulations including a background radiation field. Notation as in Fig. 2.

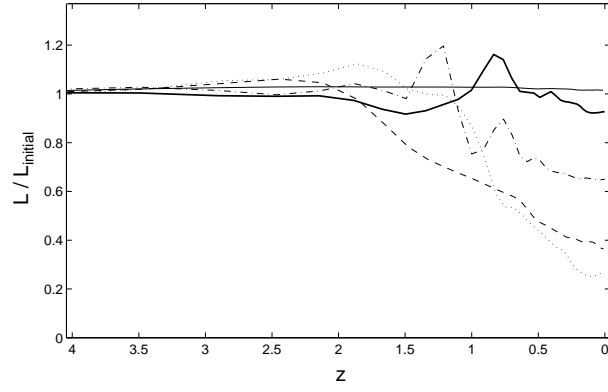


Fig. 8. Total angular momentum of the gas component, normalized to the initial value, as a function of redshift, for the simulations with a background UV field. Notation as in Fig. 2.

function of redshift. The difference is modest for the more massive galaxies, when comparing with the corresponding curves for the simulations without a background field. In the $10^{12}M_{\odot}$ simulation the fraction of hot gas at $z = 0$ increases from around 10% to 20%, when the background radiation field is included. On the other hand, the smallest galaxies show dramatic changes. In the 10^9M_{\odot} simulation, most of the gas is heated to temperatures above the virial temperature by photo-ionization. This prevents the gas from falling into the galactic halo potential well. When the background field falls in strength, after $z = 2$, about 10% of the gas is able to cool and condense into a galactic object.

The reduced cooling rate in this series of simulations, with a background UV field, also reduces the gas mass of the most massive objects that form. As can be seen when comparing Fig. 7 with Fig. 2, the reduction in object masses is most pronounced in the smallest simulations, with a total mass of 10^9M_{\odot} and $10^{10}M_{\odot}$.

There is less mass in the clumpy and cold gas component when a background UV field is incorporated. This lowers the

angular momentum transfer to the dark matter component, as can be seen in Fig. 8, to be compared with Fig. 5.

In all cases, the cold collapsed gas is concentrated in a compact object with an extent of less than a few smoothing lengths. Around this object is a second gas component in the form of a hot pressure supported halo. In the simulations where most of the gas can cool and condense into an object, most of the angular momentum is transferred to the dark matter component. In the cases where cooling is less efficient, more angular momentum is retained in the gas component, but instead the gas angular momentum is contained in the hot gas halo. The resulting gas cores are still very compact, as can be seen in Fig. 9.

6. Simulations with an ionizing field and metal enrichment

The cooling rate of interstellar gas depends sensitively on the composition assumed. Metals can increase the cooling rate by an order or two of magnitude in the temperature range relevant here. This increase is mostly due to collisional line cooling by oxygen and carbon. We employ a very simplistic scheme to estimate the metallicity of the gas, as described earlier in this paper. We have included the effects of this modulation of the

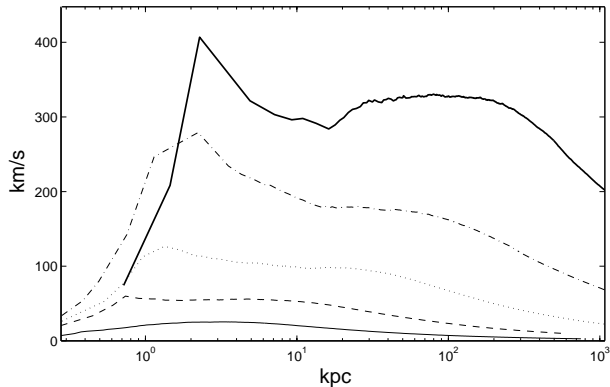


Fig. 9. Circular velocity as a function of radius, for the simulations with a background UV field. Notation as in Fig. 2.

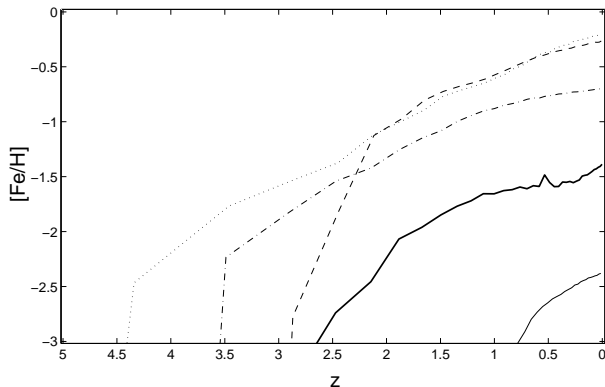


Fig. 10. Metallicity as a function of redshift. The values are the logarithm of the metal content normalized to the solar value. Notation as in Fig. 2.

gas cooling rate, in addition to the inclusion of a background radiation field. To some extent these two processes are expected to counteract each other, since a background field limits the ability of the gas to cool, and a high metal content increases the cooling rate. However, the effects of a background radiation field vanishes at low redshifts, whereas the metal content of the gas is only significant at lower redshifts, after significant star formation has taken place.

Through the amount of collapsed gas it is possible to get a very rough estimate of the star formation rate, and, with the further assumption of instant mixing, consequently an estimate of the metal enrichment. Metallicity as a function of redshift is displayed in Fig. 10, for the different simulations. The gas in the $10^9 M_\odot$ simulation does not reach metallicities high enough to significantly affect the gas cooling rate, and the result for this mass is therefore practically identical to that of the corresponding simulation without metal enrichment.

The early time evolution, for $z > 2$, is almost unchanged for all simulated proto-galaxies, when comparing with the simulations that include a background field, but no metal enrichment. At later times, the metallicity of the gas leads to more efficient cooling, as can be seen when comparing Fig. 11 with Fig. 6. A hot halo of gas, at $z = 0$, is only present in the $10^{12} M_\odot$ and

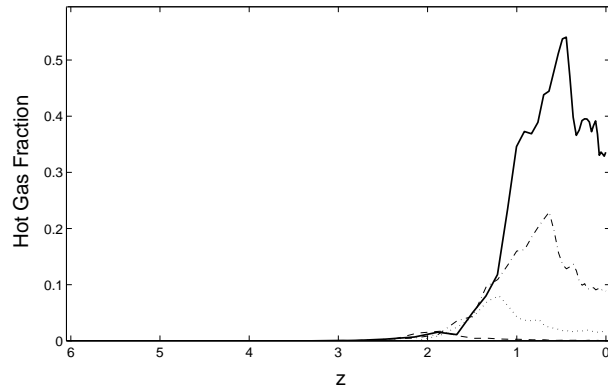


Fig. 11. The mass fraction of gas inside the virial radius that has a temperature exceeding half the virial temperature, for the simulations with a background UV field and metal enrichment. These curves are for the simulations including a background radiation field, and metal enriched gas. Notation as in Fig. 2.

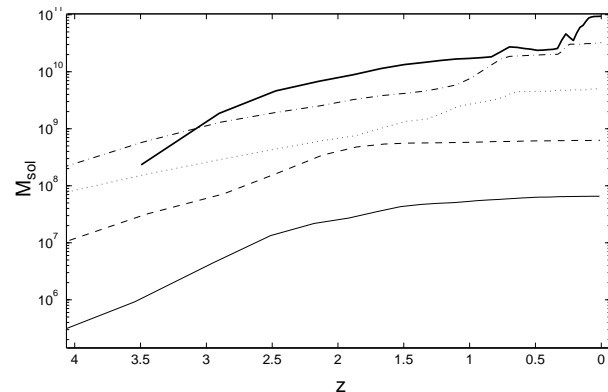


Fig. 12. The mass of the most massive progenitor, as a function of redshift, for the simulations with a background UV field and metal enrichment. Notation as in Fig. 2.

$10^{13} M_\odot$ simulations, and, in fact, all galactic halos contain less gas at virial temperatures than in the corresponding simulations without a background field and metal enrichment. The gas mass of the most massive progenitor is displayed in Fig. 12.

7. Conclusions

The mass of the most massive progenitor as a function of redshift, for all the simulations presented here, is shown in Figs. 15, 16, 17, 18, and 19.

These simulations clarify some points of previous arguments about galaxy formation that are based on simple analytic models, and estimates of the efficiency of gas cooling. It is clear that the inclusion of a background radiation field, consistent with the observed Gunn-Petersson effect, can strongly suppress the formation of galaxies with total mass less than $\approx 10^9 M_\odot$ (circular velocity < 30 km/s). Furthermore, the formation of galaxies with total mass less than $\approx 10^{10} M_\odot$ (circular velocity < 60 km/s) may be significantly delayed. These results of course depend on the assumed temporal and spectral form of the

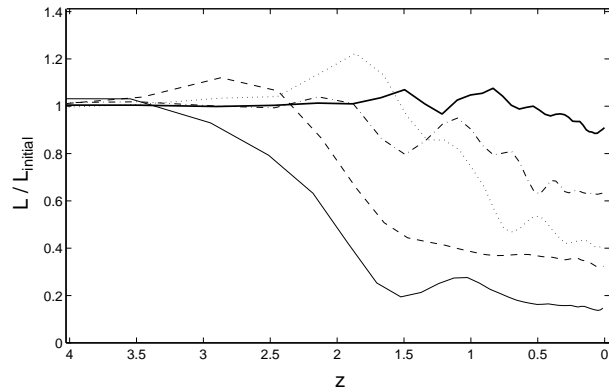


Fig. 13. Total angular momentum of the gas component, normalized to the initial value, as a function of redshift, for the simulations with a background UV field and metal enrichment. Notation as in Fig. 2.

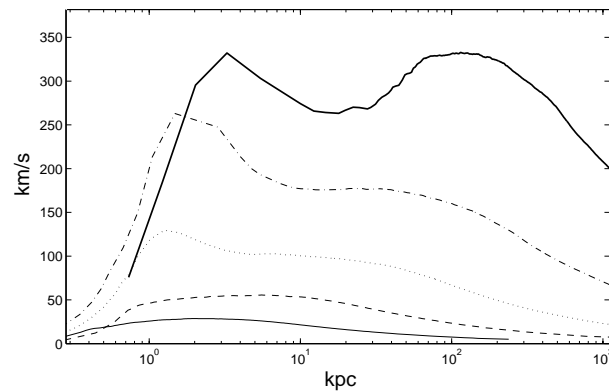


Fig. 14. Circular velocity as a function of radius, for the simulations with a background UV field and metal enrichment. Notation as in Fig. 2.

background radiation field. Nevertheless, the results are in reasonable agreement with previous analytic estimates (Efstathiou 1992), and in good agreement with recently published results based on simulations (Quinn et al. 1996, Navarro & Steinmetz 1997, Weinberg et al. 1997).

Hierarchical models of galaxy formation tend to overproduce galaxies with circular velocities less than 100 km/s. Our results indicate that photo-ionization alone is not sufficient to suppress the formation of these galaxies, since the effects on galaxies with circular velocities larger than ≈ 60 km/s is very limited.

The galactic objects that form in three-dimensional hydrodynamical simulations, are too compact when compared with observed disk galaxies. The reason for this is that most of the angular momentum in the gas component is transferred to the dark matter. Navarro & Steinmetz (1997) find that collapsed objects acquire even less angular momentum, when the effects of a UV field is included. Comparing Fig. 5 and Fig. 8, these simulations show that the angular momentum transfer, from the gas to the dark matter, decreases in magnitude when a UV field is included. This is not a contradiction. When a UV field is included, most of the gas angular momentum at $z = 0$ is contained in a hot pressure supported halo. The angular momentum content of

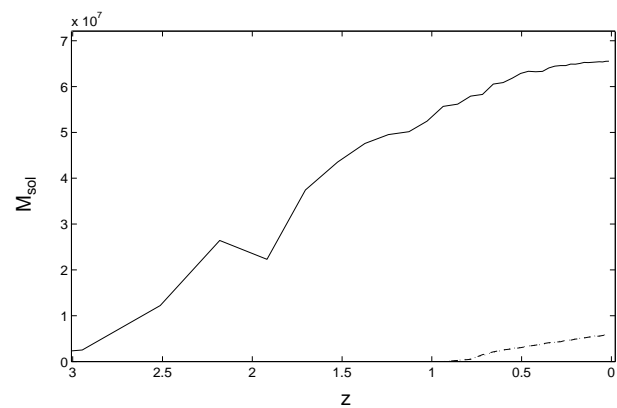


Fig. 15. Mass of the most massive progenitor, as a function of redshift. The three different curves represent values for the $10^9 M_{\odot}$ simulation, evolved in time with each one of the three physical models employed primordial gas (solid), primordial gas and background radiation field (dashed), metal enriched gas and background radiation field (dotted). On this scale, the curves for the simulations including a background UV field, with and without metal enrichment, coincide. Note that the curves represent the collapsed gas mass, the mass of the dark matter halo is not included.

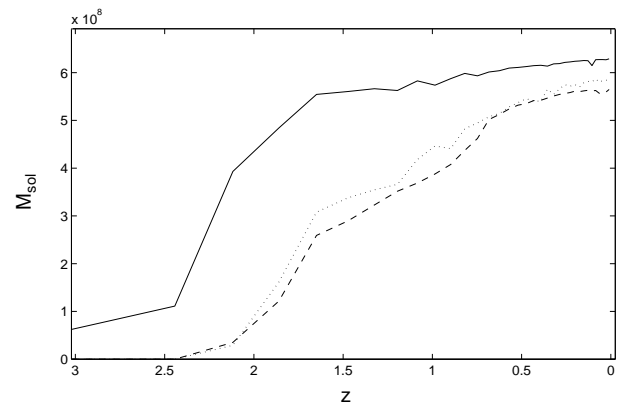


Fig. 16. Mass of the most massive progenitor, as a function of redshift. The three different curves represent values for the $10^{10} M_{\odot}$ simulation. Notation as in Fig. 15. Note that the curves represent the collapsed gas mass, the mass of the dark matter halo is not included.

the collapsed gas cores does in fact decrease also in our simulations, in agreement with the results of Navarro & Steinmetz (1997).

Metal enrichment of the interstellar gas increases the gas cooling rate at late times, and may have significant effects on the amount of gas that may cool and sink to the center of a galactic halo in a Hubble time. The inclusion of a background radiation field leads to more massive hot halos in large galaxies, 10^{12} and $10^{13} M_{\odot}$, as seen when comparing Fig. 6 with Fig. 3. These hot halos contain most of the gas angular momentum. Metal enrichment increases the gas cooling rate at late times, and could potentially lead to the collapse of the hot halo gas, to the center of the galactic dark matter halo, in a cooling flow. However, as seen in Fig. 11, the increase in cooling rate is not enough for this to happen. See however Appendix A.2 for potential two body

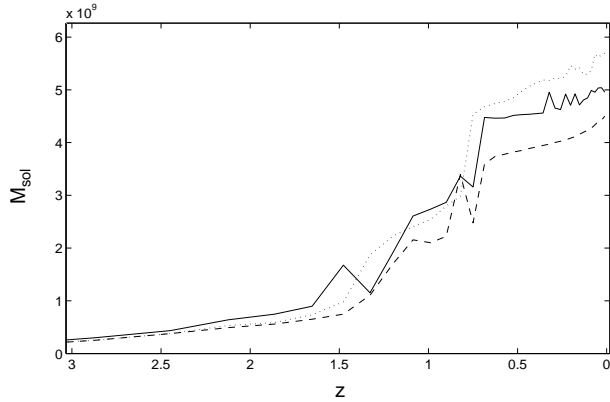


Fig. 17. Mass of the most massive progenitor, as a function of redshift. The three different curves represent values for the $10^{11} M_{\odot}$ simulation. Notation as in Fig. 15. Note that the curves represent the collapsed gas mass, the mass of the dark matter halo is not included.

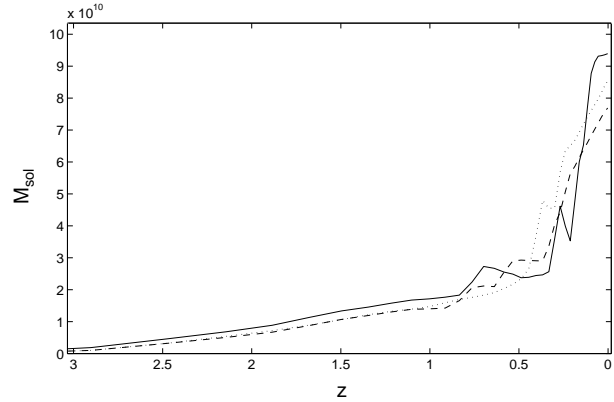


Fig. 19. Mass of the most massive progenitor, as a function of redshift. The three different curves represent values for the $10^{13} M_{\odot}$ simulation. Notation as in Fig. 15. Note that the curves represent the collapsed gas mass, the mass of the dark matter halo is not included.

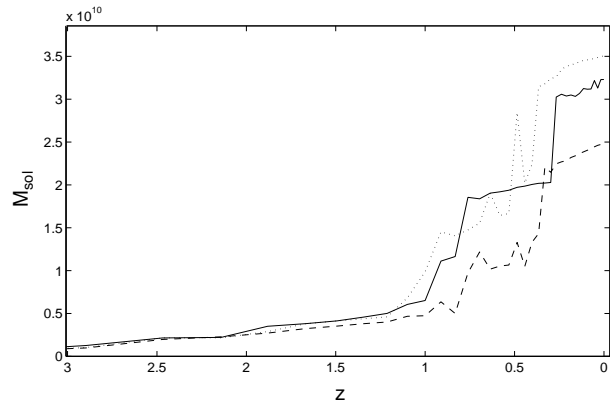


Fig. 18. Mass of the most massive progenitor, as a function of redshift. The three different curves represent values for the $10^{12} M_{\odot}$ simulation. Notation as in Fig. 15. Note that the curves represent the collapsed gas mass, the mass of the dark matter halo is not included.

heating effects. Increased cooling due to metal enrichment does decrease the mass of the hot halo that forms, (Fig. 11), but most of the gas angular momentum still resides in the remaining hot halo.

If inhomogeneities in the gas are smoothed out by the limited resolution used, the average cooling rate in the region will change. This is a problem common to all hydrodynamical simulations of galaxy formation. Some implicit assumption must be made, e.g., that the density field is smooth on unresolved scales due to physical processes not incorporated into the simulation or, that the density in regions where this could have an effect is already so high that the cooling is extremely efficient both with and without unresolved density fluctuations. Previous simulations *without* UV background ionization and heating, did *not* suffer from resolution effects, as badly as one might (naively) expect from the squared density dependence of the cooling function. The reason being that the cooling function is divided by the density, i.e. the gas cooling rate, per unit mass, is (roughly) proportional to the density, when thermal energy is integrated.

For example, Navarro & White (1994) varied the gas mass-resolution by a factor of two, and Hultman & Källander (1997), by a factor of ten, both showing comparatively small effects.

Then, when a UV background field is included, there is a competition between density vs. density squared dependencies, being explicitly sensitive to resolution. Indeed, this was observed by Weinberg et al. (1997). Varying the mass-resolution by a factor of eight, had severe effects on the outcome of their results. Navarro & Steinmetz (1997) performed similar simulations varying the mass-resolution of identical runs with a factor of six. They found much smaller effects, that in addition decreased with redshift. However, the mass-resolution was *much* higher than in Weinberg et al. (In fact, even the lower resolution runs of Navarro & Steinmetz had slightly higher resolution as compared to the “high resolution” runs of Weinberg et al.) For the simulations presented here, the absolute resolution varies, since it is proportional to the total mass, but for comparison the $10^{12} M_{\odot}$ runs are of comparable resolution to those of Navarro & Steinmetz. All in all, this is reassuring but not conclusive evidence that effects from limited numerical resolution are small. Ultimately, the tenacity of the underlying assumptions must be judged by comparisons with observations, and with other models that make different simplifying assumptions.

Acknowledgements. We are grateful to the theoretical astrophysics group, at Uppsala Astronomical observatory, in particular for providing us with the computational resources needed.

Appendix

A.1. Initial density fields

In hierarchical clustering models, structure forms by the gravitational growth of small inhomogeneities in the density field. The fluctuations in the density are conveniently characterised by the density contrast

$$\delta(\mathbf{x}) = \frac{\rho(\mathbf{x}) - \rho_b}{\rho_b}. \quad (\text{A1})$$

where ρ_b is the mean density of the universe. In an Einstein-de Sitter universe, a region with a mean density contrast of zero is marginally bound by gravity. Regions of space where the density contrast is positive are bound and will eventually collapse. At early times $|\delta| \ll 1$ and gravitational dynamics can be handled by linear theory. The mathematical formulation for this is laid out in detail by Bardeen et al. (1986), BBKS henceforth.

To single out sites where objects of mass M are likely to form, the density contrast is first smoothed on the corresponding length scale

$$\delta_s(\mathbf{x}) = \int \delta(\mathbf{x}') W_s(|\mathbf{x}' - \mathbf{x}|) d^3x'. \quad (\text{A2})$$

where

$$W_s(|\mathbf{x}|) = \exp\left(-\frac{\mathbf{x}^2}{2s^2}\right) / (2\pi s^2)^{3/2}. \quad (\text{A3})$$

s is the smoothing length scale and is given by $s \approx (M/\rho_b)^{1/3}$. If $\delta(\mathbf{x})$ is a Gaussian random field then $\delta_s(\mathbf{x})$ is also a Gaussian random field. The power spectrum of $\delta_s(\mathbf{x})$ is given by $P_s(k) = P(k) \exp(-s^2 k^2)$, where

$$P(k) \equiv \langle |\delta_k|^2 \rangle, \quad (\text{A4})$$

and δ_k is the Fourier transform of the density contrast, and $\langle \dots \rangle$ is the mean value. A peak in the field $\delta_s(\mathbf{x})$ is a point where the mass inside a spherical region of size s has a maximum. Such points are plausible sites for the formation of objects of mass M .

Hoffman et al. (1992) extended the formalism of BBKS to investigate the influence of the background density field on a given smaller scale peak. By proceeding in a similar manner we consider two Gaussian random fields, a peak field δ^p , and a background field δ^b , which are defined by their power spectra

$$P^p(k) = \begin{cases} 0 & k < k_{lim} \\ P_s(k) & k > k_{lim} \end{cases} \quad (\text{A5})$$

and

$$P^b(k) = \begin{cases} P_s(k) & k < k_{lim} \\ 0 & k > k_{lim} \end{cases} \quad (\text{A6})$$

The combined field $\delta^p + \delta^b$ is statistically identical to $\delta_s(\mathbf{x})$, the density contrast smoothed on a scale s . By requiring that $\frac{2\pi}{k_{lim}} \gg s$, extremum points in $\delta_s(\mathbf{x})$ will also be extrema of δ^p . When smoothing on galactic scales, maxima in the density field are assumed to be progenitors of galaxies.

Dimensionless field values, ν , are conveniently expressed in units of σ , i.e., $\nu = \delta/\sigma$, where

$$\sigma^2 \equiv \int P(k) \frac{4\pi k^2 dk}{(2\pi)^3} \quad (\text{A7})$$

is the mean square density contrast (BBKS). Galaxies are believed to form around peaks of height $1 < \nu < 3$, assuming the density field has been smoothed on an appropriate galactic scale. Specifying an equivalent value ν_b for the background field, at the same point, determines the density field in a larger

surrounding of the peak. ν_s , ν^p and ν^b , are related by (Hoffman et al. 1992)

$$\nu_s \sigma_s = \nu^p \sigma^p + \nu^b \sigma^b. \quad (\text{A8})$$

Inside radius s , the statistical properties of the density field are primarily determined by the small scale peak constraint. But, further away from the peak, the statistical properties depends on the value of ν^b . The main effect of the background field is to change the overall density in the vicinity of the smaller scale peak.

The approach then, is to set up a density field $\delta(\mathbf{x})$, with the constraint that the corresponding field $\delta_s(\mathbf{x})$ should have a maximum at the center of the simulated region. The small scale field δ_s is constrained by

$$\delta_s(0) = \nu^p \sigma^p. \quad (\text{A9})$$

To ensure that the field has an extremum at the center, it is also required to have vanishing first derivatives there. These constraints specifies the statistical properties of the field. The second derivative of the field could also have been used as a constraint, to ensure that the central extremum is in fact a maximum. This is neglected since it would be a largely redundant constraint. It is very unlikely that a $\nu^p \approx 2$ extremum, as is the case here, is a minimum, and therefore the statistical properties of the field are only marginally affected by adding the contrary as a constraint.

Hoffmann & Ribak (1992) showed how to create a random realization of a Gaussian field, that is subject to constraints that are linear in the field. The method is computationally efficient, and it is easy to handle several constraints. Any quantities, or combinations of, that can be represented within linear theory, can be used as constraints for the field. In addition to the ‘‘seeding’’ peak itself, we have found it useful to also specify $v(0) = 0$, i.e. requiring that the ‘‘peak’’ is stationary. This increases the likelihood that the forming object stays in the center of the simulation volume.

The field is set up in a cubic region of size L_{cube} , where $L_{cube} \gg s$. The largest wavelengths that can be represented is therefore $2\pi/L_{cube}$. The values used for s are shown in Table A1. The smoothed density field is then split into δ^b and δ^p , in such a way that δ^p contains all wavelengths that can be represented in the cube, and δ^b contains all longer wavelengths.

The background field cannot be accurately represented inside the cubic region, where the density field is constructed, since it consists of modes with wavelengths exceeding the size of the region. These long wavelength modes can still have important dynamical effects, because, by changing the overall density inside the cube, these modes change the collapse times for structures in the region. A constant density contrast of $\delta_b = \nu^b \sigma^b$ was added to the region to approximate the lowest order effects of the background field. All wavelengths longer than the expansion volume will be assumed to give a constant shift of the density.

There is, however, by no means a one-to-one correspondence between such density peaks and the galaxies that later form (Katz et al. 1993). Objects that form when peaks collapse

Table A1. Simulation parameters.

Total mass [M_{\odot}]	r_{init} [Mpc]	ν^p	ν^b	L_{cube} [Mpc]
10^9	0.15	2.0	2.0	2.0
10^{10}	0.33	2.0	2.0	4.0
10^{11}	0.71	2.0	2.0	8.0
10^{12}	1.52	2.0	2.0	16.0
10^{13}	3.27	3.0	3.0	32.0

at a high redshift can at later times merge with other collapsed objects, and form new, more massive, objects. Peaks in the density field at a high redshift will then not be in a one to one correspondence with the galaxies that later form. This is a nonlinear dynamical process that cannot be handled by linear theory. N-body calculations have shown that a significant number of the galactic halos that form, do in fact correspond to peaks in the early density field. It may be argued that the “peaks formalism” would generate atypical initial conditions. This should not be the case however, as long as the parameters are within statistically reasonable limits, i.e. $\nu \leq 3 - 4$. The generated field would still be a statistically typical one.

The gravitational particle smoothing used in the simulations are shown in Table A1.

A.2. Two-body heating

There have been recent results showing that there can be undesired, artificial heating of the gas component, due to two-body relaxation like effects, caused by the dark matter halo (Steinmetz & White 1997). This could be the case for our simulations, where the dark matter particles are of higher mass. (i.e. the simulations of 10^{12} and $10^{13}M_{\odot}$ total mass.) The effect would be that, e.g., the cooling flow might be reduced. In the hot gas halo, the cooling times are on the other hand very long, as can be seen from Fig. A1, and it cannot cool within a Hubble time. Corresponding temperatures are shown in Fig. A2. Only in the absolute center, (i.e. the disk), the cooling times are short. A few particles just within 10 kpc seems to be possibly prevented from cooling, so we cannot rule out that there are some two-body heating effects. We doubt, however, that a large fraction hot gas halo, is being held at virial temperatures, (or was formed), solely due to two-body effects. However, we believe these two-body heating effects should be taken seriously, and avoided in future work.

References

Bajtlík S., Duncan R.C., Ostriker J.P., 1988, *apj* 327, 570
 Bardeen J.M., Bond J.R., Kaiser N., Szalay A.S., 1986, *ApJ*304, 15
 Bechtold J., 1994, *ApJS*, 91, 91
 Barnes J., Efstathiou G., 1987, *ApJ*, 319, 575
 Cole S., Aragon-Salamanca A., Frenk C.S., Navarro J.F., Zepf S.E., 1994, *MNRAS*, 271, 781
 Dekel A., Silk J., 1986, *ApJ*303, 39
 Efstathiou G., 1992, *MNRAS*, 256, 43

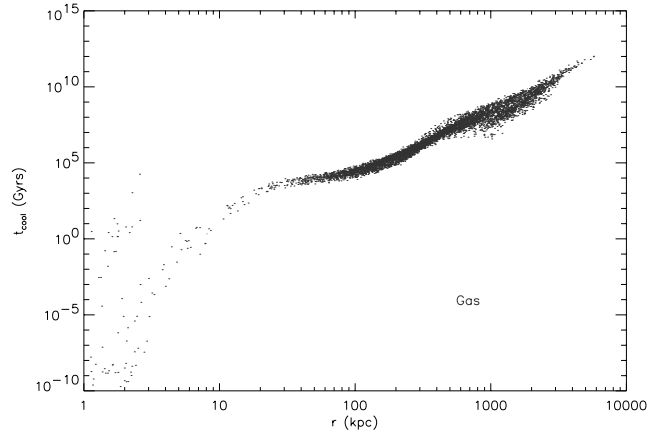


Fig. A1. Cooling times at $z = 0$, for the $10^{13}M_{\odot}$ run with metallicity. This simulation has the shortest cooling times, making potential two-body heating effects easier to detect. (There’s equally long or longer cooling times in the $10^{12}M_{\odot}$ run. Some particles in the center, have longer cooling times. This is because they have temperatures below the “drop”, $T \sim 10^4$ K, in the cooling function, and therefore have essentially no cooling.)

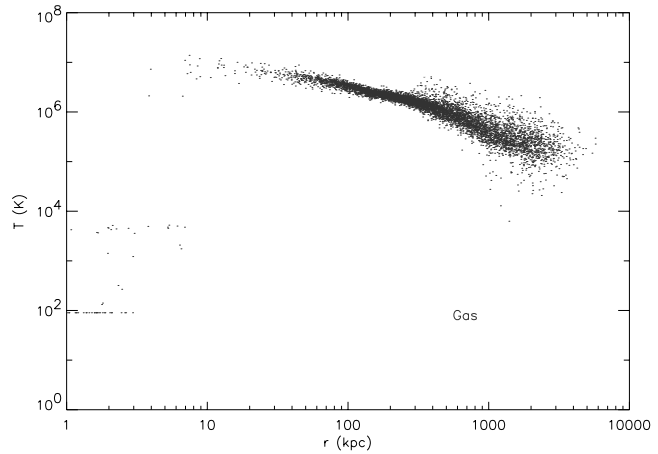


Fig. A2. Temperature at $z = 0$, for the $10^{13}M_{\odot}$ run with metallicity.

Espey B.R., 1993, *ApJ*411, L59
 Ferland G.J., 1993, in University of Kentucky Department of Physics and Astronomy Internal Report
 Haardt F., Madau P., 1996, *ApJ*461, 20
 Hoffman Y., Ribak E., 1992, *ApJ*384, 448
 Hoffman Y., Silk J., Wyse R.F.G., 1992, *ApJ*388, L13
 Hultman, J., & Källander, D. A., 1997, *A&A*324, 534
 Katz N., Gunn J.E., 1991, *ApJ*377, 365
 Katz N., Quinn T., Gelb J.M., 1993, *MNRAS*, 265, 689
 Källander, D. A., 1996 Computational Galaxy Formation Phd thesis, Uppsala university, 1996.
 Lake G., Carlberg R.G., 1988, *AJ* 96, 1581
 Lu L., Wolfe A.M., Turnshek D.A., 1991, *ApJ*367, 19
 Navarro J.F., Benz W., 1991, *ApJ*380, 320
 Navarro J.F., White S.D.M., 1994, *MNRAS*, 267, 401
 Navarro J.F., Frenk C.S., White S.D.M., 1995, *MNRAS*, 275, 56
 Navarro J.F., Steinmetz M., 1997, *ApJ*478, 13
 Quinn T., Katz N., Efstathiou G., 1996, *MNRAS*, 278, 49
 Rees M.J., 1986, *MNRAS*, 218, 25

- Rees M.J., Ostriker J.P., 1977, MNRAS, 179, 541
Silk J., 1977, ApJ211, 638
Steinmetz M., White S.D.M., 1997, MNRAS, , 288, 545
Sutherland R.S., Dopita M.A., 1993, ApJS88, 253
Tinsley B.M., 1980, in Fundamentals of Cosmic Physics 5, 287
Thoul A.A., Weinberg D.H., 1996, ApJ465, 608
Vedel H., Hellsten U., Sommer-Larsen J., 1994, MNRAS, 271, 743
Warren M.S., Quinn P.J., Salmon J.K., Zurek W.H., 1992, ApJ399, 405
Webb J.K., Barcons X., Carswell R.F., Parnell H.C., 1992, MNRAS, 257, 11
Weinberg D.H., Hernquist L., Katz N., 1997, ApJ477, 8
White S.D.M., Frenk C.S., 1991, ApJ379, 52
Williger G.M., Baldwin J.A., Carswell R.F., Cooke A.J., Hazard C., Irwin M.J., McMahon R.G., Storrie-Lombardi L.J., 1994, ApJS428, 574